Macromolecules
ARTICLE

Macromolecules **2009**, *42*, 5741–5744 **5741**
DOI: 10.1021/ma900794t

Polymer Crystallization in Nanocomposites: Spatial Reorganization of Nanoparticles

Jamil Khan,[†] Shane E. Harton,[†] Pinar Akcora,[†] Brian C. Benicewicz,[‡] and Sanat K. Kumar*[,†]

[†]*Department of Chemical Engineering, Columbia University, New York, New York 10027, and* [‡]*Department of Chemistry, University of South Carolina, Columbia, South Carolina 29208*

Received April 11, 2009; Revised Manuscript Received June 13, 2009

ABSTRACT: The crystal sizes and melting points of polyethyleneoxide, crystallized in the presence of silica nanoparticles, are only affected for particle loadings larger than 20 wt %. X-ray scattering shows that the distribution of particle spacings in the semicrystalline state is always significantly broader than in the melt, even though the mean particle spacing is unchanged. We thus conclude that, at low loadings, the polymer "forces" the nanoparticle "defects" out of their way to crystallize in a minimally perturbed form. For higher loadings, the crystals become smaller in response to increased particle induced confinement. In contrast to currently held views that the particles control the crystallization process, e.g., by providing heterogeneous nucleation sites, we find that the crystalline lamellae dominate; i.e., they manipulate the nanoparticle dispersion, especially at low loadings.

1. Introduction

There has been considerable interest in polymer crystallization[1−4] in confined spaces, e.g., in thin films and in the presence of sheet-like fillers.[2,3] These situations are thought to be analogous and the type of crystal formed, the degree of crystallinity (X_c) and melting temperature (T_m) are expected to be dramatically affected on confinement.[5−8] For example, it has been found in several cases that the presence of a planar surface, which serves as a nucleation site, tends to increase the rate of crystallization. Similarly, recent work has shown that the presence of spherical nanoparticles yields whole new crystal morphologies. While we are interested in understanding how the presence of nanoparticles might affect the semicrystalline morphologies, more pertinently we ask how the crystallization of these polymers affects the spatial distribution of nanoparticles. We ask this question since it is now very well appreciated that the macroscopic properties of nanocomposites are strongly affected by the dispersion state of nanoparticles.[9,10] However, since the particles used in most previous studies are very large (or are strongly agglomerated), the particle dispersion state is not affected by the crystallization of the polymer. We conjectured that this situation must change for nonagglomerated nanoscale particles, such as the ones we consider here.

2. Experimental Methods

Bare, unfunctionalized silica particles (nominally 15 ± 4 nm in diameter) were obtained as dispersions in methylethylketone from Nissan Chemicals. Both TEM and SAXS determined form factors independently confirm the bare particle sizes.

PMMA ($M_w = 31.0$ kDa; $M_w/M_n = 1.06$) brushes were grown from the surfaces of these silica nanoparticles using RAFT polymerization as outlined elsewhere.[11,12] The SiO_2-*g*-PMMA had a grafting density of 0.27 chains/nm^2, as determined using thermogravimetric analysis (TGA). The unperturbed radius of gyration of these chains is ∼4.7 nm. We use dynamic light scattering (DLS) to measure the thickness of the brushes, since SAXS has too little contrast between the brush and solvent to give an accurate estimate of the brush thickness. Since these DLS measurements only make sense in a small molecule solvent, where the brush sizes are different from that in the melt state, we do not quote the DLS determined brush results here, but defer them to a separate paper. Regardless, it is important to stress that our results in good solvent show that the brush heights are comparable to single (ungrafted) chain dimensions in the same solvent. These brush chains are thus not significantly swollen relative to their ungrafted counterparts. PEO ($M_w \sim 100$ kDa) was purchased from Scientific Polymer Products and used as received. The glass transition temperatures (T_g) of the PMMA in the nanoparticle brush and pure PEO were determined using modulated DSC (see below) to be 110 and −55 °C, respectively. The T_g of the PMMA implies a somewhat atactic triad distribution.[13]

To prepare the nanocomposites, PEO and SiO_2-*g*-PMMA were individually dissolved in benzene (>99%, Sigma Aldrich) at *ca.* 80 °C. After complete dissolution of each, several filler loadings (corresponding to 0, 10, 20, 40, and 60% w/w SiO_2−PMMA) were prepared by mixing various ratios of the two solutions. The solutions were sonicated using a probe sonicator for 3 min and poured into PTFE drying dishes and allowed to dry overnight in a fume hood. A word is in order here about the role of sonication: we have previously reported that probe sonication (for the times and power used in this work) does not lead to a significant change in particle hydrodynamic radius. More recently, our collaborators, Drs. Vaia and Koerner (Wright Patterson Air Force Base) have examined how sonicating particle solutions affect the brush coatings. In their experiments, the particle size stays constant and very little (<2%) free polymer appears for short sonication times (<15 min). For longer times, the apparent particle size (as determined by DLS) decreases, and a proportionately larger amount of free polymer, presumably cleaved from the particle surface, appears. Thus, the sonication process, under the conditions we employ, only disperses the particles without changing them.

After drying in the fume hood, the nanocomposites were annealed *in vacuo* (∼10^{-3} Torr) for 24 h at 80 °C. According to a Stokes−Einstein analysis of the SiO_2−PMMA particle diffusivity,[14] using previously reported values for the PEO viscosity,[15,16] this was sufficient time to allow the SiO_2−PMMA

*Corresponding author. E-mail: sk2794@columbia.edu.

Published on Web 07/14/2009

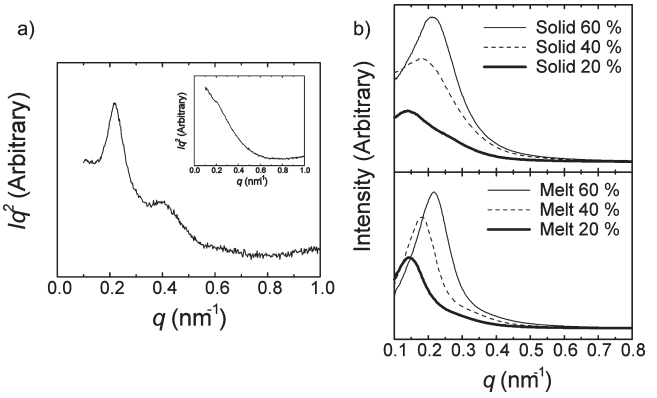

Figure 1. (a) Lorentz-corrected SAXS of semicrystalline PEO as a function of the scattering vector, q. From here, the lamellar thickness was determined to be 25 nm. The inset in part a shows the Lorentz-corrected SAXS for pure PEO after 45 min at 80 °C. (b) Analysis of the nanocomposites below T_c (top, at room temperature) and above T_m (bottom, at 80 °C), after background subtraction, reveals negligible changes in the effective nanoparticle spacing (average confinement of 19, 10, and 4 nm for 20, 40, and 60 wt % filler loading, respectively), but a broadened distribution in nanoparticle spacings is apparent below T_c. This has been further quantified from the effective halfwidth-at-half-maximum (Δq) on the high-q side of the peaks ($\Delta q = 0.06$, 0.05, and 0.05 nm^{-1} for 20, 40, and 60% loadings above T_m, respectively, and $\Delta q = 0.11$, 0.10, and 0.08 nm^{-1} for 20, 40, and 60% loadings below T_c, respectively).

particles to fully disperse. Finally, the samples were compression molded at 80 °C using a Carver press with heated platens and allowed to slowly cool (~5 °C/h) to 30 °C and were stored in a calcium sulfate-filled desiccator to minimize water absorption. Crystallization thus occurs under nonisothermal conditions.

Modulated DSC[17] was performed using an indium (temperature) and sapphire (heat capacity) calibrated TA Instruments Q100 in a nitrogen atmosphere. Approximately 10 mg of sample was placed in an aluminum sample pan, and a heating rate of 3 °C/min, a modulation amplitude of 1 °C, and a modulation period of 60 s was used. The integral heat of melting determined for the first heating cycle (−85 to +180 °C), after normalization to the PEO weight fraction, was used to determine degree of crystallinity, using the previously reported PEO heat of formation (H_f = 196.4 J/g).[18] Both the onset and peak melting temperatures ($T_{m,o}$ and $T_{m,p}$, respectively) were determined from the first heating cycle.

SAXS was performed at beamline X27C at Brookhaven National Laboratories using 9 keV photons ($\Delta E/E \approx 1.1\%$) and a detector distance of 2 m. Samples were first analyzed at 25 °C (as-molded), and then they were heated to 80 °C for 45 min and analyzed in the melt in order to assess the solid and melt dispersions of the brush-coated nanoparticles. WAXD was performed using an Inel X-ray diffractometer with 0.154 nm photons (Cu Kα radiation) over the range $4° < 2\theta < 120°$ using a multiangle detector. Analysis was performed for approximately 5 min at 25 °C for each sample.

To determine the morphology, the nanocomposites were microtomed and visualized in a Jeol JEM-100 CX electron microscope.

3. Results

We first used the self-consistent mean-field theory to substantiate our initial guess that the polymer brush thickness could be approximated by its unperturbed single chain value. Calculations[19,20] for a SiO_2-*g*-PMMA/PEO blend with a binary mean-field interaction parameter $\chi = -0.001$,[10] shows that the brush thickness is $\sim 1.1 R_g \sim 5$ nm (where R_g is the PMMA chain radius of gyration) in good agreement with our conjecture. Thus, the net effective diameter of a grafted nanoparticle is ~ 15 + 5 + 5 nm =25 nm. Using modulated DSC[17] the onset and peak of the melting

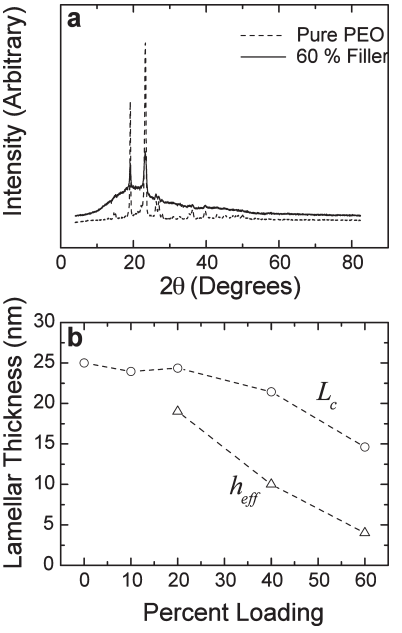

Figure 2. (a) WAXD results showing negligible changes in the monoclinic crystalline lattice spacing for pure PEO and PEO with 60% filler. (b) We used a Scherrer analysis of the (120) reflection at $2\theta \cong 19°$ to determine the lamellar thickness (L_c) as a function of filler loading. This is compared to the SAXS-determined surface-to-surface nanoparticle spacing ($h_{eff} = 2\pi/q_m - d_{eff}$, where d_{eff} is the effective particle diameter, 25 nm). Clearly, the lamellar thicknesses and surface-to-surface nanoparticle spacings do not coincide.

isotherm ($T_{m,o}$ and $T_{m,p}$) for the pure PEO were determined to be 58 and 67 °C, respectively. The crystallization temperature (T_c) of PEO was determined to be *ca.* 45 °C for a 5 °C/min cooling cycle (no modulation).

The results from Lorentz-corrected small-angle X-ray scattering (SAXS)[21] of the pure PEO are shown in Figure 1a. From the first-order maximum (q_m) at 0.22 nm^{-1}, the lamellar thickness was determined using

$$L_{c,o} = X_{c,o}\frac{2\pi}{q_m}$$

where $L_{c,o}$ (25 nm) and $X_{c,o}$ (0.87) are the lamellar thickness and degree of crystallinity, respectively, of the pure PEO sample. These results are consistent with previously reported values for $L_{c,o}$ and $X_{c,o}$ for pure PEO of comparable molecular weight.[21−23] Figure 1b shows the SAXS results for 20, 40, and 60% (w/w) filler loadings both (top) below T_c (room temperature) and (bottom) above T_m (80 °C). Importantly, the origins of the scattering peaks in Figure 1, parts a and b, are quite different: in Figure 1a, the primary scattering contrast is between the crystal and amorphous phase (~ 10% increase in electron density for crystalline PEO over amorphous PEO), while the dominant contrast in Figure 1b is between the silica and the polymer (~ 80% increase in electron density for silica over crystalline PEO). Using the relationship

$$h_{eff} = \frac{2\pi}{q_m} - d_{eff}$$

where h_{eff} is the effective surface-to-surface separation between the particles and d_{eff} is the effective particle diameter (25 nm), h_{eff} was determined to be 19, 10, and 4 nm for 20, 40, and 60% filler loadings, respectively, in both the melt and solid state (Figure 2b). This shows a high degree of confinement for these filler loadings, with h_{eff} considerably lower than the equilibrium lamellar thickness, $L_{c,o}$. Note that the mean particle spacing (h_{eff}) is essentially unchanged when one cools a sample from the melt to below the

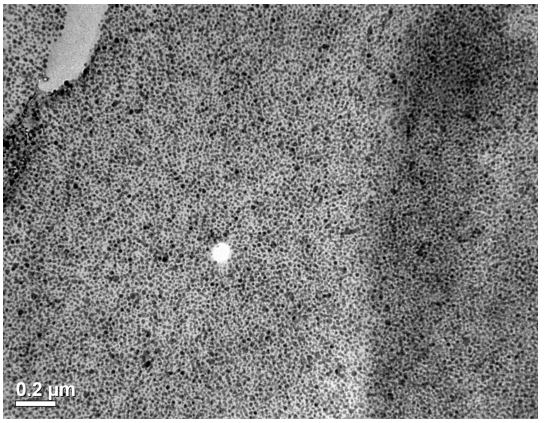

Figure 3. Transmission electron microscopy results for system comprised of 60 % of the silica. The data were taken for a sample at room temperature, thus corresponding to the crystal state.

T_c. However, since the X-ray peaks broaden in the crystalline state (Figure 1b), we conclude that the distribution of particle separations is broadened in the crystalline state: this is quantified by the effective half-width-at-half-maximum (Δq) on the high-q side of the peaks, $\Delta q = 0.06$, 0.05, and 0.05 nm^{-1} for 20, 40, and 60% loadings above T_m, respectively, while it is $\Delta q = 0.11$, 0.10, and 0.08 nm^{-1} below T_c, respectively. These results are particularly compelling for the 40 and 60% loadings, where the intensity of the interparticle structure factor (i.e., particle−particle diffraction) completely dominates the single-particle form factor intensity.[24] Transmission electron microscopy imaging (TEM) over a range of particle loadings in the crystallized state show that the particles are always uniformly distributed. Figure 3 of a representative highly filled sample (60 % SiO_2-*g*-PMMA) illustrates this point, although we hasten to add that the TEM results, which are from ∼50−100 nm thick slices, could suffer from artifacts due to two-dimensional projection effects.[25] Regardless, no obvious signs of large scale particle agglomeration are seen.

The wide-angle X-ray diffraction (WAXD) results for pure PEO and 60% filled PEO in Figure 2a show no measurable changes in the crystalline lattice structure of the PEO under confinement, meaning that a constant enthalpy of melting, H_f can be assumed for all samples. The WAXD Bragg peaks at $2q \cong 19°$, corresponding to the (120) reflection of the monoclinic lattice,[26] were fit to a Pearson function and a Lorentz function for the amorphous halo.[23,27] (We remind the reader that *b* is usually the unique direction in a monoclinic system. This justifies the use of the (120) reflection to evaluate lamellar "size".) Using the lamellar thickness for pure PEO determined using SAXS, $L_{c,o}$, these WAXD results were used to approximate PEO lamellar thicknesses, L_c in the presence of the SiO_2−PMMA, according to Scherrer's equation[28]

$$L_c \cong L_{c,o}\frac{\beta_o}{\beta}$$

where β is the full width at half-maximum of the fitted (120) peak (β_o for pure PEO). This relies on the fact that the lattice spacing is independent of filler loading, and it assumes that the instrumental resolution is negligible compared to the Scherrer-broadening for these small lamellar "grains." It is also useful to point out that the line broadening might also be due, in part or in whole, to crystal defects. Results are shown in Figure 2b and compared to the measured values of h_{eff}. While L_c values decrease somewhat with increasing loading, they are much larger than the average confinement due to the nanoparticles.

The results from the Scherrer analysis are confirmed by comparison with modulated DSC results for $T_{m,o}$ and $T_{m,p}$ as a function of filler loading with the theoretical values from the Gibbs−Thomson relationship[7]

$$T_m = T_{m,\infty}\left(1 - \frac{2\gamma_e}{L_c H_v}\right)$$

where γ_e is the PEO lamellar/amorphous interfacial tension (20 mJ/m^2),[29,30] H_v is the volumetric heat of formation (210 J/cm^3),[29,30] and $T_{m,\infty}$ is the melting temperature in the limit of infinite lamellar thickness. $T_{m,\infty}$ was adjusted to match $T_{m,o}$ and $T_{m,p}$ for the pure PEO, and the values of L_c from the Scherrer analysis were input as a function of filler loading. Figure 4a shows excellent agreement between the experimental and theoretical changes in $T_{m,o}$ and $T_{m,p}$ as a function of filler loading. However, Figure 4b shows a significant decrease in X_c at high filler loadings (∼ 40% reduction in X_c with 60% filler), indicating a preference for thicker PEO lamellae at a sacrifice of total crystallinity in the presence of nanoparticles.

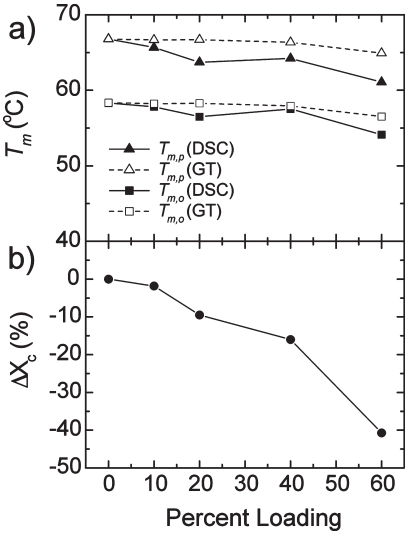

Figure 4. Experimental (DSC) and theoretical (GT) analysis of the onset ($T_{m,o}$) and peak ($T_{m,p}$) melting temperatures for PEO nanocomposites as a function of filler loading (a). The theoretical Gibbs−Thomson function was used with the measured values for L_c (see Figure 2) and previously reported parameters. This confirms the small changes in L_c determined using SAXS and WAXD. Also shown are the results for the degree of crystallinity as a function of filler loading (b). These results, coupled with the SAXS in Figure 1b, suggest that growing crystalline lamellae in highly filled nanocomposites can maneuver the particles in order to grow thicker lamellae within broaden insterstitials.

4. Discussion

For linear polymer chains, confinement to thin films has been shown to reduce T_m since lamellar sizes are restricted to be smaller than the film thickness.[5,7,8] Similarly, for side-chain crystalline polymers, it has been shown that confinement to planar thin films can significantly reduce X_c for films less than 50 nm thick, and even prevent crystallization completely below 15 nm, by kinetically confining both the side chains and the polymer backbone to a disordered state.[6,31,32] Here, a similar phenomenon could occur, although the nanocomposite system has one key difference from planar thin films. For thin films, the polymer chains cannot relieve their confinement unless the film dewets the substrate, thereby forming locally thicker domains.[33] With nanocomposites,[34] we suggest that the growing crystalline lamellae can maneuver the particles in order to grow thicker, more favorable lamellae, as schematically outlined in Figure 5. The SAXS results in Figure 1b clearly demonstrate this phenomenon which results in a broader distribution of nanoparticles below T_c. Therefore, even though the average effective confine-

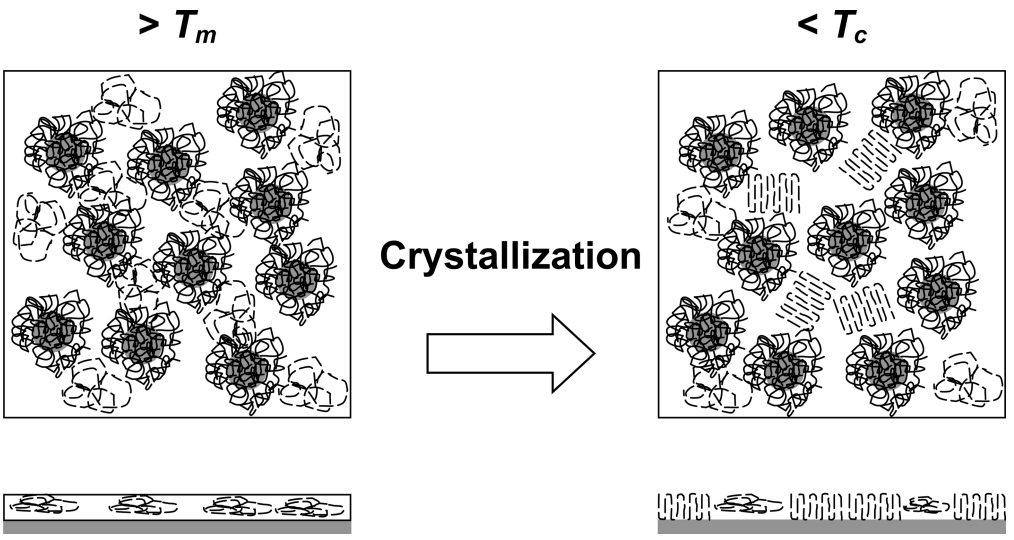

Figure 5. Crystallization in the presence of brush-coated nanoparticles (top) and confined to thin films (bottom). In well-dispersed nanocomposites, the growing lamellae can maneuver the nanoparticles, thereby broadening interstitials to allow bulk-like lamellae to form. However, in thin films where no dewetting is present, the lamellae are forced to grow with a reduced thickness. Note that we do not show all the polymer chains, which should be space-filling because we use polymer melts.

ment (d_{eff}) remains unchanged when a sample is cooled from above T_m to below T_c for highly filled semicrystalline polymer nanocomposites, the formation of lamellae are restricted to the broadened interstitials, resulting in relatively small changes in the measured lamellar thicknesses (L_c), and hence, T_m, but large decreases in the degree of crystallinity (X_c).

These results parallel the role of defects (or impurities) in the crystallization of metals and polymers: in general, the crystallization process is so thermodynamically dominant that the system will push these "defects" out of the way so as to result in a minimally perturbed crystallization process. A particularly relevant comparison here is the crystallization behavior when one considers miscible polymer blends with a crystallizable and an amorphous component. In these cases, for slow enough crystallization rates (i.e., close to the equilibrium melting point), it is found that the amorphous polymer can be completely expelled from the spherulites, emphasizing the apparent generality of this finding.

While our results thus have clear parallels to "molecular" mixtures with defects, no such phenomenon has been observed for polymer nanocomposites, especially for platelet fillers and for large micrometer sized glass beads. We attribute these results to two facts: first, these platelets or beads are much too large to be easily maneuvered by the growing lamellae. Second, these more planar fillers can facilitate the nucleation and growth of the polymer crystals, making them much more intimate participants in the crystallization process. The critical nanoparticles size where one transitions between the behavior in the presence of platelet fillers and that in the presence of nanoparticle filters remains an open and interesting question that we shall probe in future work.

References and Notes

(1) Tjong, S. C. *Mater. Sci. Eng., R* **2006**, *53*, 73–197.
(2) Bockstaller, M. R.; Thomas, E. L. *J. Phys. Chem. B* **2003**, *107*, 10017–10024.
(3) Winey, K. I.; Kashiwagi, T.; Mu, M. F. *MRS Bull.* **2007**, *32*, 348–353.
(4) Schadler, L. S.; Kumar, S. K.; Benicewicz, B. C.; Lewis, S. L.; Harton, S. E. *MRS Bull.* **2007**, *32*, 335–340.
(5) Kim, J. H.; Jang, J. S.; Zin, W. C. *Macromol. Rapid Commun.* **2001**, *22*, 386–389.
(6) Frank, C. W.; Rao, V.; Despotopoulou, M. M.; Pease, R. F. W.; Hinsberg, W. D.; Miller, R. D.; Rabolt, J. F. *Science* **1996**, *273* (5277), 912–915.
(7) Wang, Y.; Ge, S.; Rafailovich, M.; Sokolov, J.; Zou, Y.; Ade, H.; Luning, J.; Lustiger, A.; Maron, G. *Macromolecules* **2004**, *37*, 3319–3327.
(8) Wang, Y.; Rafailovich, M.; Sokolov, J.; Gersappe, D.; Araki, T.; Zou, Y.; Kilcoyne, A. D. L.; Ade, H.; Marom, G.; Lustiger, A. *Phys. Rev. Lett.* **2006**, *96*, 028303.
(9) Balazs, A. C.; Emrick, T.; Russell, T. P. *Science* **2006**, *314* (5802), 1107–1110.
(10) Ito, H.; Russell, T. P.; Wignall, G. D. *Macromolecules* **1987**, *20*, 2213–2220.
(11) Li, C.; Han, J.; Ryu, C. Y.; Benicewicz, B. C. *Macromolecules* **2006**, *39*, 3175–3183.
(12) Li, C. Z.; Benicewicz, B. C. *Macromolecules* **2005**, *38*, 5929–5936.
(13) Fuchs, K.; Friedrich, C.; Weese, J. *Macromolecules* **1996**, *29*, 5893–5901.
(14) Tuteja, A.; Mackay, M. E.; Narayanan, S.; Asokan, S.; Wong, M. S. *Nano Lett.* **2007**, *7*, 1276–1281.
(15) Colby, R. H. *Polymer* **1989**, *30*, 1275–1278.
(16) Hyun, Y. H.; Lim, S. T.; Choi, H. J.; Jhon, M. S. *Macromolecules* **2001**, *34* (23), 8084–8093.
(17) Wunderlich, B.; Jin, Y. M.; Boller, A. *Thermochim. Acta* **1994**, *238*, 277–293.
(18) Hikosaka, M. Y.; Pulcinelli, S. H.; Santilli, C. V.; Dahmouche, K.; Craievich, A. F. *J. Non-Cryst. Solids* **2006**, *352*, 3705–3710.
(19) Dan, N.; Tirrell, M. *Macromolecules* **1992**, *25*, 2890–2895.
(20) Harton, S. E.; Kumar, S. K. *J. Polym. Sci., Part B: Polym. Phys.* **2008**, *46*, 351–358.
(21) Baldrian, J.; Horky, M.; Sikora, A.; Steinhart, M.; Vlcek, P.; Amenitsch, H.; Bernstorff, S. *Polymer* **1999**, *40*, 439–445.
(22) Martuscelli, E.; Pracella, M.; Wang, P. Y. *Polymer* **1984**, *25*, 1097–1106.
(23) Homminga, D.; Goderis, B.; Dolbnya, I.; Reynaers, H.; Groeninckx, G. *Polymer* **2005**, *46*, 11359–11365.
(24) Roe, R.-J. *Macromolecules* **1986**, *19*, 728–731.
(25) Koga, T.; Takenaka, M.; Aizawa, K.; Nakamura, M.; Hashimoto, T. *Langmuir* **2005**, *21*, 11409–11413.
(26) Bortel, E.; Hodorowicz, S.; Lamot, R. *Makromol. Chem.* **1979**, *180*, 2491–2498.
(27) Lafrance, C. P.; Debigare, J.; Prudhomme, R. E. *J. Polym. Sci., Part B: Polym. Phys.* **1993**, *31*, 255–264.
(28) Huang, P.; Zheng, J. X.; Leng, S. W.; Van Horn, R. M.; Jeong, K. U.; Guo, Y.; Quirk, R. P.; Cheng, S. Z. D.; Lotz, B.; Thomas, E. L.; Hsiao, B. S. *Macromolecules* **2007**, *40*, 526–534.
(29) Godovsky, Y. K.; Slonimsk, Gl *J. Polym. Sci., Part B: Polym. Phys.* **1974**, *12*, 1053–1080.
(30) Calahorra, E.; Cortazar, M.; Guzman, G. M. *Polymer* **1982**, *23*, 1322–1324.
(31) Despotopoulou, M. M.; Miller, R. D.; Rabolt, J. F.; Frank, C. W. *J. Polym. Sci., Part B: Polym. Phys.* **1996**, *34*, 2335–2349.
(32) Despotopoulou, M. M.; Frank, C. W.; Miller, R. D.; Rabolt, J. F. *Macromolecules* **1996**, *29*, 5797–5804.
(33) Massa, M. V.; Carvalho, J. L.; Dalnoki-Veress, K. *Phys. Rev. Lett.* **2006**, *97*, 247802.
(34) Muthukumar, M. *Eur. Phys. J. E* **2000**, *3*, 199–202.